Visualization of Compression and Spillover in a Coadsorbed System: Syngas on Cobalt Nanoparticles

Emily A. Lewis,[†] Duy Le,[‡] April D. Jewell,[†] Colin J. Murphy,[†] Talat S. Rahman,[‡,*] and E. Charles H. Sykes[†,*]

[†]Department of Chemistry, Tufts University, Medford, Massachusetts 02155-5813, United States, and [‡]Department of Physics, University of Central Florida, Orlando, Florida 32816, United States

ABSTRACT Competitive adsorption and lateral pressure between surface-bound intermediates are important effects that dictate chemical reactivity. Lateral, or two-dimensional, pressure is known to promote reactivity by lowering energetic barriers and increasing conversion to products. We examined the coadsorption of CO and H_2, the two reactants in the industrially important Fischer–Tropsch synthesis, on Co nanoparticles to investigate the effect of two-dimensional pressure. Using scanning tunneling microscopy, we directly visualized the coadsorption of H and CO on Co, and we found that the two adsorbates remain in segregated phases. CO adsorbs on the Co nanoparticles *via* spillover from the Cu(111) support, and when deposited onto preadsorbed adlayers of H, CO exerts two-dimensional pressure on H, compressing it into a higher-density, energetically less-preferred structure. By depositing excess CO, we found that H on the Co surface is forced to spill over onto the Cu(111) support. Thus, spillover of H from Co onto Cu, where it would not normally reside due to the high activation barrier, is preferred over desorption. We corroborated the mechanism of this spillover-induced displacement by calculating the relevant energetics using density functional theory, which show that the displacement of H from Co is compensated for by the formation of strong CO–Co bonds. These results may have significant ramifications for Fischer–Tropsch synthesis kinetics on Co, as the segregation of CO and H, as well as the displacement of H by CO, limits the interface between the two molecules.

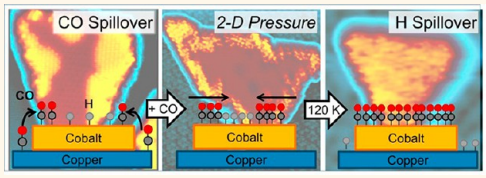

KEYWORDS: CO · H_2 · lateral compression · overlayer compression · Fischer–Tropsch synthesis

Molecular adsorption, dissociation, interaction, and reaction are key steps in all heterogeneously catalyzed processes. Molecular binding to the active metal surface defines a potential energy landscape that in turn dictates the preferred adsorption geometries of subsequent adsorbates. It has been shown in simple systems like benzene on Pd(111) that, as the benzene surface coverage is increased, lateral interactions between the molecules cause the initially flat-lying benzene to tilt in order to accommodate higher surface coverage.[1,2] The loss in binding energy to the surface in the high-coverage, tilted state is compensated for by the formation of a greater number of molecule–surface bonds. These effects can be thought of in terms of a lateral, or two-dimensional, pressure between the molecules, which leads to a change in their adsorption orientation. This change in overlayer structure yields additional space for more molecules to bind per unit area, subsequently lowering the effective two-dimensional pressure.

Two-dimensional pressure also plays a role in mixed systems and affects chemical reactivity. In studies of the trimerization of acetylene to benzene on Pd(111), the newly formed benzene adsorbs on the surface in two states: a loosely bound, tilted species that is compressed by unreacted acetylene on the surface, and a tightly bound, flat-lying conformation that forms as more space becomes available through the reduction in acetylene coverage by reaction.[3−5] The selectivity of the trimerization reaction toward benzene can be improved by the adsorption of a spectator molecule, NO, which reduces the available sites for acetylene adsorption, forcing the latter into a compressed state and eliminating the formation of decomposition products.[6] Crucially, during this reaction, the acetylene and NO molecules are not thought to directly interact and remain segregated in different domains on the

* Address correspondence to Talat.Rahman@ucf.edu, charles.sykes@tufts.edu.

Received for review February 22, 2013 and accepted April 5, 2013.

Published online April 08, 2013
10.1021/nn400919y

surface, with NO acting solely as a spectator that serves to raise the two-dimensional pressure on the surface.

A number of surface science studies have examined the effect of coadsorption of various adsorbates on model surfaces, revealing that segregation and compression are prevalent effects that influence both diffusion and reaction. Notably, although most of these investigations have been carried out in ultrahigh vacuum (UHV), several have been corroborated by high-pressure[7,8] or macroscale[9] measurements and a few studies have been performed with high-pressure scanning tunneling microscopy (STM),[8,10,11] confirming that the effects of segregation have ramifications on reaction kinetics under catalytically relevant conditions. A number of reports have investigated the coadsorption of CO and H on Pd(111), and it has been shown that there are repulsive interactions between the species.[7,12,13] The CO and H form compressed, segregated domains on the Pd surface,[7,12−14] and with increasing CO coverage, H is forced to desorb or absorb into subsurface Pd sites, depending on specific conditions.[7,12,13] In related works, Salmeron and co-workers observed the compression of O by H on Pd(111)[15,16] and demonstrated that the strain of this compression is relieved by H dissolution into the bulk.[16]

CO and O are also known to form segregated domains on both Pd(111)[17] and Pt(111),[9] and CO was shown to compress O on these surfaces due to its stronger adsorption energy. This segregation effect limits the CO oxidation reaction on Pt(111) to the interface between the species, and the rate law developed from this nanoscale observation was corroborated by macroscale measurements.[9] High pressure STM studies have shown that the coadsorption of CO can also affect mobility in catalytic systems, as it can block adsorption sites and limit diffusion of reactants.[8,10] It was demonstrated that the adsorption of CO on Pt(111) suppresses H−D exchange at room temperature by blocking the H_2/D_2 dissociation sites and decreasing H/D mobility on the Pt surface.[8] A similar study illustrated that CO poisons the ethylene hydrogenation reaction on Pt(111) and Rh(111) by blocking active sites and inducing the formation of dense, mixed domains of the adsorbates that are unable to diffuse on the surface.[10] Another high-pressure STM study examined CO and NO segregation on Rh(111) as a function of their partial pressures. Coadsorption at low NO partial pressure led to the formation of large mixed CO−NO domains, whereas coadsorption at high standing NO pressure caused segregated NO islands to nucleate as a result of like-molecule interactions.[11] Recently, Tysoe and co-workers studied the activation energy barrier in the acetoxylation of ethylene to vinyl acetate over Pd(111).[18] They first calculated this value experimentally, and then modeled the system theoretically. It was found that the only way to obtain a theoretical activation barrier that matched the experimentally derived value was to take into account an acetate-saturated surface in which the electronic structure of the intermediates is altered at high acetate coverage.

These studies demonstrate that a dramatic effect on the interaction, mixing, and mobility of reactants occurs upon coadsorption on catalytic surfaces, and that these complex interactions can affect activation energies and, hence, reaction activities and selectivities. Our goal was to investigate these complex interactions in syngas, a mixture of CO and H_2, which can include the impurities CO_2 and H_2O due to the competing reverse water−gas shift reaction.[19] Syngas is the feedstock for the industrially important Fischer−Tropsch synthesis (FTS) process used to make liquid hydrocarbons. Co is a common catalyst for this reaction, but it undergoes a phase change and refacets during typical surface science cleaning procedures. We therefore investigated the coadsorption of H_2 and CO, the two major components of syngas, on the close-packed surface of well-defined Co nanoparticles grown on an inert Cu(111) substrate. This approach enables us to examine the close-packed surface of Co, as well as mimic the highly stepped nature of a nanoparticle.[20]

It was previously calculated that the coadsorption of CO on Co should destabilize adsorbed H, as well as intermediates resulting from H-assisted CO dissociation,[21−23] and it was suggested that further investigation into the effect of coadsorbed species could help elucidate the carbon insertion mechanism.[24] We have investigated the coadsorption of CO and H on Co with low temperature (LT) STM and density functional theory (DFT). We found that H and CO remain segregated on model Co nanoparticle surfaces and that the spillover of CO onto the nanoparticles displaces H *via* two-dimensional pressure, initially compressing it and eventually forcing it to spill over onto the Cu(111) support. We visualized both the metastable, compressed state of H on Co and the transition to the thermodynamically preferred state in which H spills over onto the Cu support and CO occupies all available sites on Co. Our DFT calculations allow us to quantify the energetics of both of these steps. We suggest that the observed segregation, compression, and displacement effects could have kinetic ramifications for FTS, given that reaction between CO and H must occur at interface sites between H and CO.

RESULTS AND DISCUSSION

The growth of Co on Cu(111) yields well-defined bilayer triangular Co nanoparticles that dissociatively adsorb H_2.[20,25−31] It is generally accepted that the majority of the Co at low coverage follows the FCC stacking of the underlying Cu substrate, and thus, the major exposed surface of Co is the (111) facet.[26,27,32] These Co nanoparticles have been extensively studied

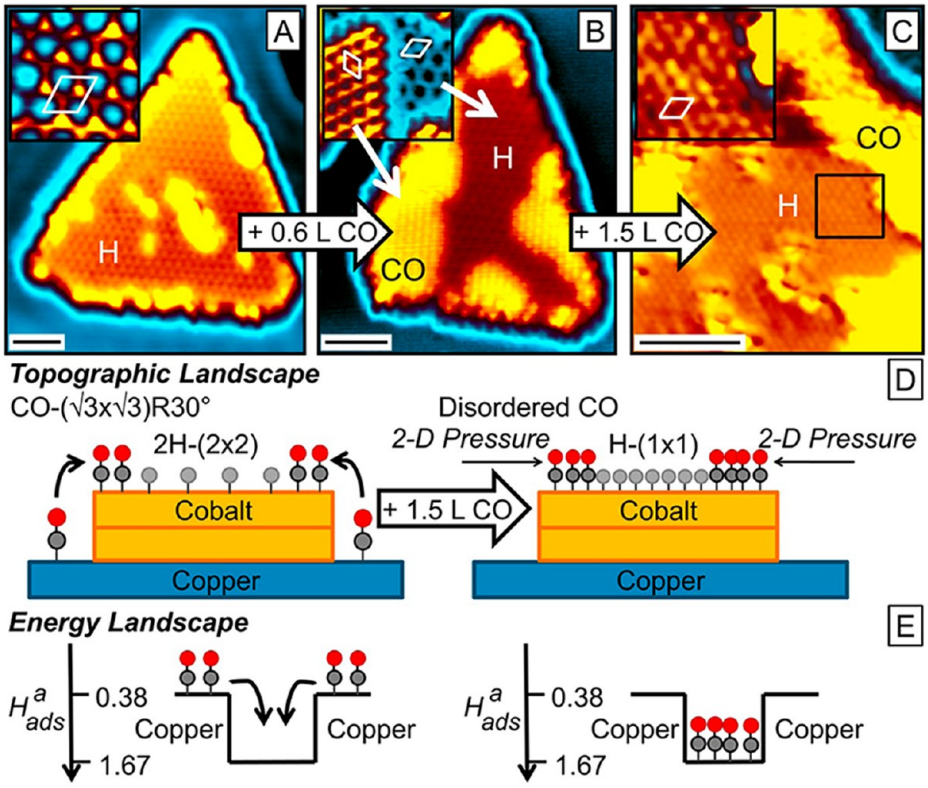

Figure 1. STM images illustrating CO spillover-induced two-dimensional compression of H on Co nanoparticles at 78 K. All scale bars = 3 nm. (A) Co nanoparticle with adsorbed H in the 2H-(2 × 2) low-coverage phase. The bright spots at the edges of the nanoparticle are likely CO molecules that have been adsorbed from the background of the chamber. Inset (2.13 × 2.13 nm^2): Unit cell of the 2H-(2 × 2). (B) Co nanoparticle with both CO (protrusions) and H (depressions) adsorbed on the surface. Inset (2.73 × 2.73 nm^2): High resolution STM image at the interface of the H and CO domains. The unit cells of the CO-(√3 × √3)R30° (left) and 2H-(2 × 2) (right) phases on the surface are shown by the white rhombuses. (C) Co nanoparticle after compression of H by addition of more CO. Inset: High-resolution image of the area shown in the box illustrating the H-(1 × 1) unit cell. (D) Side-view schematic of the compression of H on the Co nanoparticles on Cu, where the left side is analogous to (B) and the right side is analogous to (C). (E) DFT- parametrized energy landscape for CO spillover from Cu to Co.

for their interesting magnetic properties.[33−36] They also provide an excellent substrate for bridging the structure gap between Co single crystals and catalytic nanoparticle surfaces, given that Co nanoparticles <20 nm have an FCC structure.[20,37,38] We have previously examined dissociative H_2 adsorption on these model Co nanoparticle surfaces with STM and have demonstrated three coverage (θ) dependent phases of atomic H on the Co surface: at $\theta \approx 0.5$ ML a 2H-(2 × 2) unit cell is preferred (Figure 1A inset), at $\theta \approx 0.67$ ML a less common 6H-(3 × 3) structure forms, and at $\theta \approx 1$ ML a H-(1 × 1) structure is prevalent (Figure 1B inset).[20] The formation of the latter two phases is attributed to the step edges of the Co nanoparticle, in accordance with previous predictions,[39] and in the case of the H-(1 × 1) phase, the Co−Cu interface may provide an additional low-energy pathway for the dissociation and spillover of H. Although a majority of our surfaces are Co(111), a similar saturation H coverage is expected for Co(0001) and Co(100),[39] and we do not see a difference in any of the effects reported here between the faulted and unfaulted triangles. In addition to the H phases, we are also able to image two of the known ordered phases of CO on Co(0001) on the Co nanoparticles: the low coverage a CO-(√3 × √3)R30° and the high coverage 7CO-(2√3 × 2√3)R30°.[40,41] The images shown in Figure 1 demonstrate the effect of CO-induced lateral pressure on the H overlayer structure. Figure 1A shows a Co nanoparticle that is covered with the 2H-(2 × 2) adlayer. Upon adsorption of 0.6 L (L, 10^{-6} Torr·s) of CO on the same system, it can be seen (Figure 1B) that both adsorbates are now present on the Co, with the CO predominantly occupying sites near the edges and the H residing in the center of the nanoparticle. At this coverage, both CO and H exist in their lowest density ordered structures, CO-(√3 × √3)R30° and 2H-(2 × 2), as indicated by the unit cells in the inset of Figure 1B. Upon depositing an additional 1.5 L of CO on the same surface, there is a marked difference in the ordering of the adsorbates; the CO structure becomes more dense and disordered, similar to what has been previously observed for CO in confined systems,[42,43] and the H overlayer is compressed to the H-(1 × 1) structure (Figure 1C). The schematic in Figure 1D illustrates this effect of two-dimensional compression of H by CO.

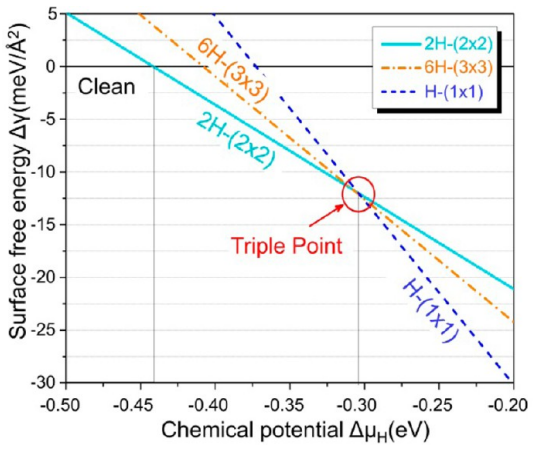

Figure 2. Surface free energies of different H phases on Co nanoparticles as a function of hydrogen chemical potential, revealing a transition between 2H-(2 × 2) and H-(1 × 1) structures and a triple point (circled) that includes a 6H-(3 × 3) phase.

It is interesting to note that we always observe the segregation of H and CO on the Co nanoparticles, irrespective of whether the adsorbates are sequentially dosed or simultaneously coadsorbed. This is contrary to what might be expected, as CO and H are known to form a homogeneous phase on Ni(111).[44] Given that FTS proceeds by coadsorption of CO and H on the catalytic particles, this result is important and indicates that the interface length between the regions of CO and H may be a critical descriptor for reactivity; similar results have been reported by Ertl and co-workers for the catalytic oxidation of CO on Pt(111).[9]

We explain the mechanism for CO adsorption on Co *via* direct adsorption onto the Co nanoparticle and also through spillover from the Cu support, which further leads to compression of the H overlayers by CO around the edges of the Co nanoparticle. Since the sticking probability of CO on Cu is ~0.9 at 105 K,[45] it is expected that the Cu will become populated with CO concurrently with the Co nanoparticles. We observe, however, that the Cu terrace begins to populate only after the CO has become fully compressed and disordered on Co and the compressed H-(1 × 1) phase is present on the Co surface, supporting the mechanism of spillover of CO from Cu to Co. This spillover is represented schematically in Figure 1D along with the energetic landscape (Figure 1E) that drives this behavior. These DFT calculations will be described in detail later. CO adsorbs with similar probability on the whole surface but is thermodynamically driven to occupy any available site on the Co particles. At 78 K, CO can diffuse on Cu and adsorbs at the edges of the Co nanoparticles. This facile spillover is what ultimately leads to the lateral compression of the H overlayers on Co.

Our calculations based on DFT give insight into the energetics of the compression of H by CO. The simplified phase diagram of the hydrogen-adsorbate structures on Co/Cu(111) is illustrated in Figure 2 and shows the dependence of the surface free energy of the examined surfaces on the hydrogen chemical potential, $\Delta\mu_H$.[20] As the chemical potential of H increases, the minimum of surface free energy occurs first with the clean Co surface, then with the 2H-(2 × 2) structure, and finally with the H-(1 × 1) structure. This implies the transition from the clean Co/Cu(111) surface to the 2H-(2 × 2) phase at medium and to the H-(1 × 1) phase at high chemical potential. Interestingly, there is a triple point at which the 2H-(2 × 2), 6H-(3 × 3), and H-(1 × 1) intersect. This result elucidates the transitory nature of the 6H-(3 × 3), as the limited range of $\Delta\mu_H$ would suggest difficulty in achieving the phase, which is presumably why we have never observed it as a product of compression.

TABLE 1. DFT Data[a]

	E_{ads} [eV]	H^a_{ads} [J m^{-2}]
Co/Cu(111)		
CO-($\sqrt{3} \times \sqrt{3}$)R30°	1.22	1.14
7CO-($2\sqrt{3} \times 2\sqrt{3}$)R30°[b]	1.02	1.67
H-(2 × 2)	0.49	0.34
2H-(2 × 2)	0.50	0.70
6H-(3 × 3)	0.46	0.87
H-(1 × 1)	0.43	1.19
Cu(111)		
CO-($\sqrt{3} \times \sqrt{3}$)R30°	0.41	0.38
H-(2 × 2)	0.18	0.13
2H-(2 × 2)	0.19	0.27

[a] E_{ads} is binding energy per CO molecule or per H atom (including zero-point motion correction), and H^a_{ads} is the adsorption energy footprint, or adsorption energy per unit area, of the species. [b] The structure is adopted from ref. [48]

The mechanism of CO spillover and H compression can also be thought of, not in terms of the absolute binding strength of each adsorbate to Co, but with adsorption energy "footprints" on the Co surface, which we denote as H^a_{ads} (Table 1).[46] This descriptor takes into account the adsorption energy per unit surface area that each species occupies. The term is analogous to spreading pressure, which is the change in surface free energy of a solid substrate upon adsorption of a vapor.[47] Adsorption energies, E_{ads}, of CO and H on Cu(111) and Co/Cu(111) were also calculated within our DFT framework (Table 1). The fact that the H^a_{ads} for CO on Co is much higher than H^a_{ads} for CO on Cu corroborates CO's preference for population of the Co nanoparticles. Using these values for H^a_{ads}, we calculate that compressing 1 mol of H atoms from the 2H-(2 × 2) structure to the H-(1 × 1) structure with CO spilled over from Cu to Co is exothermic by 25 kJ.

The two-dimensional compression of H by CO was further studied using time-lapse STM imaging (movies) taken over a ~1 h time span. These movies, depicted as individual frames in Figure 3, show the stark contrast in the mobility of the adsorbates in the low CO coverage system compared to the high-coverage, compressed

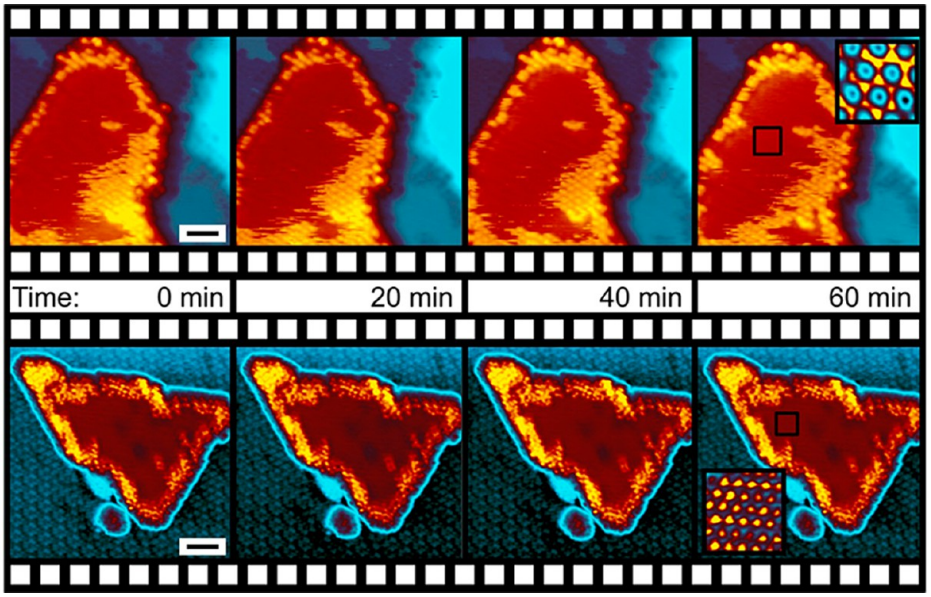

Figure 3. Frames from two time-lapse STM movies. Imaging was performed under identical scanning conditions at 78 K (Scale bars = 2 nm). Top: Coadsorbed CO (bright) and H (dark areas) that are not compressed and mobile. Inset: (1.66 × 1.66 nm^2) 2H-(2 × 2) in the nanoparticle center that is not readily visible. Bottom: Coadsorbed CO and H in the immobile, compressed system. Inset: (1.30 × 1.30 nm^2) High-resolution image of the H-(1 × 1).

system. The top panels show the uncompressed system and demonstrate that the H atoms and CO molecules are mobile. The CO in its uncompressed ($\sqrt{3} \times \sqrt{3}$)R30° phase is able to freely diffuse over the Co nanoparticles, as the low density 2H-(2 × 2) phase continually shifts its location to accommodate. It is important to note that even throughout this thermally driven diffusion process, the molecules always remain segregated in homogeneous domains on the Co surface, which indicates that the phase separation is a thermodynamically driven process. The lower panels in Figure 3 show the compressed system in which densely packed CO surrounds the central H-(1 × 1) region. From this series of images, it is clear that there is no mobility in this compressed system, as the position of each CO molecule remains fixed over time. Importantly, both of these movies were taken under identical STM imaging conditions and surface temperature. Unlike the 2H-(2 × 2) structure that has vacancies in the overlayer, the H-(1 × 1) structure leaves no vacant sites into which mobile molecules or atoms can diffuse, and compression, induced by the tightly packed CO, locks the adsorbates in place.

To explore the full extent of the compression of H by CO on Co, we examined the system at 5 K, a temperature at which H can be imaged on the Cu(111) surface. We first deposited H onto the 5 K Co/Cu(111) system, forming a 2H-(2 × 2) overlayer on the Co nanoparticles. We then deposited CO onto this sample, and it was observed that H largely blocks CO uptake on the Co surfaces at this temperature, as only small areas of CO are present on the nanoparticles (Figure 4A). It was also seen that CO populates the Cu terrace, which we confirmed by taking time-lapse images (Figure 4A inset). We are able to distinguish CO from H on Cu(111) by their distinct diffusion rates. At 5 K and scanning at nonperturbative conditions (<50 pA, < 50 mV), H diffuses rapidly on the Cu(111) surface due to quantum tunneling.[49] CO is very tightly bound on the Cu surface at 5 K and does not diffuse until very aggressive scanning conditions are employed (pulses >4.5 V). Thus, by scanning at nonperturbative conditions, CO and H can be easily distinguished by their diffusion rates. To explore the effect of CO pressure on H overlayers, we annealed the sample shown in Figure 4A to ~120 K, which resulted in the system displayed in Figure 4B. The CO originally on the Cu terrace has compressed the H on the Co nanoparticle to its less favorable H-(1 × 1) phase and displaced additional H that could not fit in the reduced area. The displaced H, unable to desorb from the Co nanoparticle at 120 K, is forced to spill over onto the Cu(111) terrace (Figure 4B inset). To the best of our knowledge, this is the first direct visualization of compression-induced spillover of an adsorbate from a nanoparticle to the support.

To further investigate compression-induced spillover, we deposited a high coverage of H_2 on the Co/Cu(111) surface at 80 K to obtain the H-(1 × 1) structure, as formation of the H-(1 × 1) phase on Co is activated and will not occur at 5 K.[20] We then cooled the sample down to 5 K to allow for H imaging on the Cu. A typical nanoparticle resulting from this preparation is shown in Figure 5A, where it is seen that the Co is mostly populated with the H-(1 × 1) overlayer. A small amount of CO is present around the Co edges due to adsorption from the background during the cool down procedure. There is additional CO on the Cu(111)

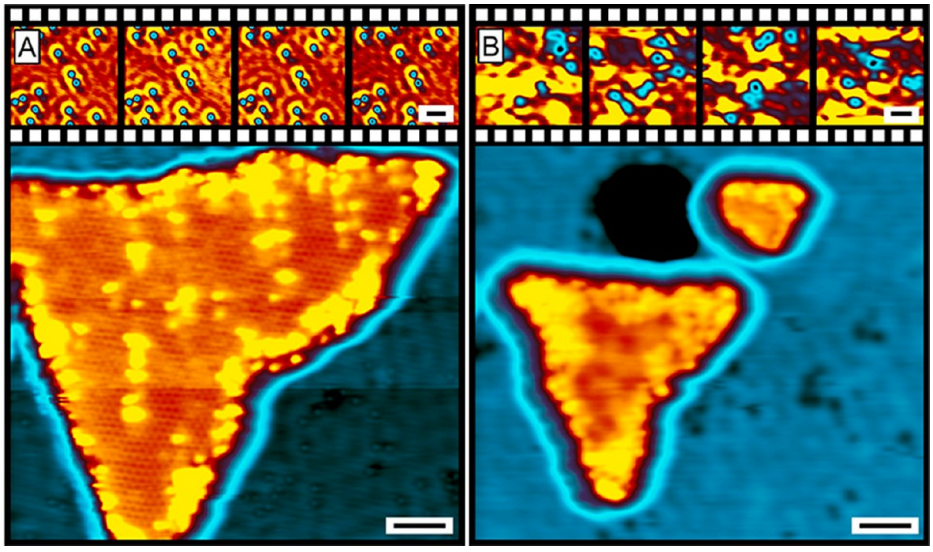

Figure 4. STM images illustrating compression-induced spillover. Scale bars = 3 nm. The insets in each panel are time-lapse movies taken on the Cu surface, with ~6 min between each consecutive frame. Scale bars = 2 nm. (A) Image showing a Co nanoparticle covered with the 2H-(2 × 2) structure, as well as a small amount of CO (bright protrusions). A low coverage of CO is also present on the Cu(111) terrace. The insets depict CO on the Cu terrace that is immobile over the movie length (~18 min). (B) Image showing the same system following a ~120 K anneal. The CO now extensively covers the Co nanoparticles, forming a dense disordered phase. The H is compressed to the H-(1 × 1) structure, as indicated by the presence of the dark defect triangles on the Co surface.[20] Most interestingly, H atoms are now present on the Cu terrace, indicative of induced spillover from Co. The insets show the diffusion of H on the Cu terrace over ~18 min.

terrace, which appears as immobile depressions. Similar to the aforementioned experiment, we annealed this system to ~120 K, and again the CO displaced the H from the Co nanoparticle (Figure 5B). This time, due to the large concentration of CO on the Cu terrace, CO was able to fully displace H on the Co nanoparticles.

Again, by examining our H^{a}_{ads} values presented in Table 1, it is clear that the phenomenon of reverse spillover is driven by the stronger preference of CO to bind to Co *vs* Cu, and the energy lost in having the H spill over from Co to the Cu surface is compensated for by the energy gained in having the CO bind to Co. Using the H^{a}_{ads} data, we find that displacing 1 mol of H atoms in the H-(1 × 1) phase from Co to Cu with CO is exothermic by 11 kJ. Additionally, the occurrence of this full reverse spillover indicates that the initial compression of H by an excess of CO is a metastable state that, once given enough thermal energy, equilibrates to the thermodynamically preferred arrangement where only CO occupies the available Co surface area and H is present on the Cu. Thus, we have been able to visualize and energetically explain both the thermodynamic product of H−CO exchange on Co and an intermediate, compressed state that we have thermally isolated. While we acknowledge the "pressure−temperature gap" between our experiments and FTS which takes place at ~200 °C and 25 bar, there is no current way to probe these phenomena with this fine level of detail using *in situ* techniques. Given the high density of our adlayer structures, we expect that both the preferential binding of CO *vs* H to Co and the segregation we observe should occur at higher pressures. Furthermore,

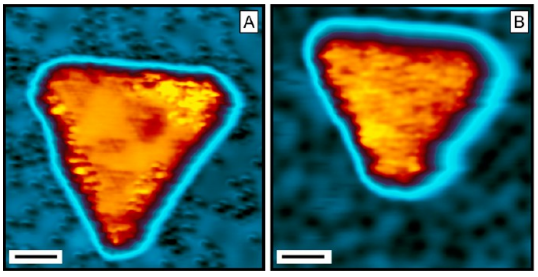

Figure 5. STM images demonstrating the spillover of H from Co nanoparticles to the Cu surface induced *via* spillover of CO from Cu to Co (Scale bars = 2 nm). The system in (A) was prepared by dosing H_2 on the Co nanoparticles at 80 K to obtain the H-(1 × 1), then cooling the sample to 5 K. Although the H-(1 × 1) structure is not well-resolved, the presence of the triangular defects in the overlayer is indicative of the phase.[20] The bright protrusions at the top right corner of the Co nanoparticle are coadsorbed CO molecules. On the Cu(111) terrace, the CO images as disordered depressions. The surface shown in (B) is the result of annealing the system in (A) to ~120 K. It is apparent that the H-(1 × 1) structure no longer exists on the Co surface and that it has been replaced by disordered CO. The H, which images as mobile depressions on Cu, has spilled over from the Co onto the Cu surface.

the calculated adsorption energies and surface free energies include vibrational contributions, making them relevant at higher temperatures. Although some deviations in the calculated energetics may come about with coadsorption of molecules, as expected at ambient pressures, the differences in the binding energy of CO superstructures to the Co and Cu surfaces are sufficiently large to indicate qualitative preservation of the trends obtained here for reactions carried out under more realistic, industrial conditions. Thus, this reverse

spillover has interesting ramifications for adsorbate interactions on supported catalytic nanoparticles, as strong segregation forces and adsorption site preferences keep the species in exclusive domains on the nanoparticle surface and can lead to spillover of the weaker-bound species to the support, making for complex reaction kinetics.

CONCLUSIONS

Using scanning tunneling microscopy and density functional theory calculations, we have demonstrated the spillover-induced compression and compression-induced spillover of H by CO on model Co nanoparticles. These effects offer new insight into the microscopic details of the interaction of the reactants of Fischer–Tropsch synthesis, whereby the segregation of H and CO forces them to interact at their domain interfaces either on the nanoparticle surface or at the nanoparticle-support boundary. Furthermore, since many high-coverage overlayers can only be formed at high standing pressures, specifically three-dimensional pressures, our result of inducing a higher coverage phase through spillover-induced two-dimensional pressure has exciting ramifications for studying high two-dimensional pressure systems in UHV. Given the balance between binding energy and molecule–molecule repulsion, there should be a range of two-dimensional pressures under which many important overlayer systems restructure and compress in response to the addition of a second more strongly binding adsorbate. Additionally, the compression-induced spillover of adsorbates to less preferred binding sites provides interesting opportunities to study industrially important reactants on catalytic surfaces that are not typically feasible under UHV conditions like H on Cu. This gives surface scientists an opportunity to study unique, catalytically relevant adsorbate phases with a wide range of analytical tools.

MATERIALS AND METHODS

Experimental Section. STM imaging was carried out in UHV using an Omicron NanoTechnology GmbH low temperature scanning tunneling microscope at 78 or 5 K, as noted in the text. The Cu(111) crystal (MaTecK) was prepared by first sputtering with Ar^+ (1 kV/14 μA) then annealing to 1000 K in a separate preparation chamber ($P = 2 \times 10^{-10}$ mbar). Following cleaning, the sample was transferred to the STM chamber ($P = 1 \times 10^{-11}$ mbar) where it was cooled to cryogenic temperature within ~1 h. Cobalt depositions were performed on a room temperature sample in the preparation chamber using a Focus GmbH EFM3 electron beam evaporator with a flux ~0.05 ML min^{-1}, resulting in Co coverages of 20–35%. The sample was returned to the precooled scanning stage (<5 min) following the deposition to prevent intermixing of Co and Cu. Line-of-sight molecular dosers installed on the STM chamber enabled the precision deposition of CO and H_2 (Airgas, 99.99% and 99.999%, respectively) onto the cooled surface. Both cut Pt/Ir and etched W tips were used to scan the sample using tunneling currents between 0.3 and 1.5 nA and voltages between ±10 and ±100 mV.

Theoretical. We carried out our *ab initio* calculations of hydrogen overlayers on the Co/Cu(111) surface using spin-polarized DFT with the plane-wave pseudopotential and the projector-augmented wave (PAW)[50,51] methods, as implemented in the Vienna *Ab-initio* Simulation Package (VASP).[52] We used the generalized gradient approximation (GGA) in the form of the Perdew-Burke-Ernzerhof (PBE) functional[53] for describing the exchange-correlation of the electrons. Depending on the adsorbate-overlayer in question, we used a supercell consisting of a (1 × 1), (2 × 2), or (3 × 3) Cu(111) slab of 6 layers, which is constructed stoichiometrically from bulk Cu with the optimized lattice parameter of 3.636 Å. Two layers of Co in FCC stacking are present on one side of the Cu(111) slab. The slab is separated from its normal periodical-images by a vacuum of 20 Å. We correspondingly sampled the Brillouin zone with (13 × 13 × 1), (7 × 7 × 1), or (5 × 5 × 1) uniform k-point meshes. The kinetic energy cutoff for the wave function expansion is set to 350 eV. We performed structural relaxation until all force components acting on each atom, except for those in the bottom three Cu layers which are kept fixed at their equilibrium positions in the Cu slab, were less than 0.01 eV/Å. We used dipole correction to total energy[54] to cancel the effect of asymmetry in the slab configuration.

To build the hydrogen-overlayer phase diagram, we examined the surface free energy of the clean Co/Cu(111) surface and five hydrogen structures adsorbed on that surface: H-(2 × 2), 2H-(2 × 2), 5H-(3 × 3), 6H-(3 × 3), and H-(1 × 1). The stability of H adsorbate structures in thermal equilibrium with a reservoir (here it is H_2, and characterized by chemical potential of hydrogen μ_H) is determined by the surface free energy[55] with respect to that of the clean Co/Cu(111) surface which is defined as:

$$\Delta\gamma = \frac{1}{A}[(E_{n\mathrm{H-Co/Cu(111)}} - E_{\mathrm{Co/Cu(111)}}) + \Delta F^{\mathrm{Vib}} - n\mu_{\mathrm{H}}] \quad (1)$$

Here, $E_{\mathrm{Co/Cu(111)}}$ and $E_{n\mathrm{H-Co/Cu(111)}}$ are, respectively, the total energies of a Co/Cu(111) system with zero and n H atoms adsorbed on the Co side of the slab; A is surface area; ΔF^{Vib} is the difference in the vibrational contribution to the free energy of the two systems. In this work, we approximate ΔF^{Vib} by taking into account only the vibrational modes of the adsorbed H and Co atoms in the topmost layer. We calculated the frequencies of these modes by using the finite-difference method: each atom is displaced ±0.01 Å in each Cartesian coordinate to calculate all forces acting on each atom by using the Hellmann–Feynman theorem (the displacement of 0.01 Å maintains the validity of the harmonic approximation and avoids numerical errors that would otherwise introduce chaotic behavior in the results). From these forces, the dynamical matrix was constructed and diagonalized. At low temperatures (<200 K), the dependence of the vibrational contribution to the free energy on temperature is negligible. The surface free energy is nevertheless a function of the chemical potential, μ_H, which in turn is a function of temperature and hydrogen pressure, and is approximately defined as:

$$\mu_{\mathrm{H}} = \frac{1}{2}\left[E_{\mathrm{H_2}} + E_{\mathrm{H_2}}^{\mathrm{ZPE}} + \tilde{\mu}_{\mathrm{H_2}} + k_{\mathrm{B}}T \ln\left(\frac{p_{\mathrm{H_2}}}{p_{\mathrm{o}}}\right)\right] \quad (2)$$

where $E_{\mathrm{H_2}}$ and $E_{\mathrm{H_2}}^{\mathrm{ZPE}}$ are the total energy and the ZPE of an isolated H_2 molecule; $\tilde{\mu}_{\mathrm{H_2}}$ is its chemical potential at temperature T and pressure p_o; k_B is the Boltzmann constant, and $p_{\mathrm{H_2}}$ is the pressure of H_2 exposure. μ_H reaches a maximum value at $1/2(E_{\mathrm{H_2}} + E_{\mathrm{H_2}}^{\mathrm{ZPE}}) = -3.27$ eV, at which point H_2 molecules start to condense on the Co/Cu(111) surface. Equation 2 indicates that the chemical potential of H increases as the pressure of H_2 increases. Although we can determine the exact value for $\tilde{\mu}_{\mathrm{H_2}}$, its exact value is inconsequential because we are only concerned

with the variation of the surface free energy as a function of $\Delta\mu_H - 1/2(E_{H_2} + E_{H_2}^{ZPE})$ to evaluate the relative stability of various H overlayer structures as a function of H_2 pressure.

For systems involving CO molecules, we set the cutoff energy for the planewave expansion to 500 eV to accurately describe the C and O atoms. To overcome the overestimation of adsorption energies and DFT's tendency to predict incorrect adsorption sites of CO on Cu(111) (3-fold hollow instead of the on-top site),[56] we used the DFT+U approach.[57] Here, we found that U = 6 eV for C and O atoms, which produces an adsorption energy and adsorption site of CO on Cu(111) that are in agreement with those extracted from experimental data.[58,59] We calculated vibrational frequencies of CO molecules while keeping the Co/Cu(111) substrate frozen.

Conflict of Interest: The authors declare no competing financial interest.

Acknowledgment. The authors thank the U.S. Department of Energy (Grant Nos. FG02-10ER16170 (C. Murphy, M. Mattera., M. Liriano, E. Sykes) and FG02-07ER15842 (T. Rahman, D. Le)) for their support. T. Rahman and D. Le also acknowledge partial support from NSF Grant CHE-0741423 under which the DFT calculations had begun. E. Lewis acknowledges the Department of Education for her GAANN fellowship. A. Jewell would like to thank the National Science Foundation for a graduate research fellowship. Calculations were performed on the high performance computational facility STOKES at UCF.

REFERENCES AND NOTES

1. Tysoe, W. T.; Ormerod, R. M.; Lambert, R. M.; Zgrablich, G.; Ramirez-Cuesta, A. Overlayer Structure and Kinetic Behavior of Benzene on Palladium(111). *J. Phys. Chem.* **1993**, *97*, 3365–3370.
2. Hoffmann, H.; Zaera, F.; Ormerod, R. M.; Lambert, R. M.; Wang, L. P.; Tysoe, W. T. Discovery of a Tilted Form of Benzene Chemisorbed on Pd(111): A NEXAFS and Photoemission Investigation. *Surf. Sci.* **1990**, *232*, 259–265.
3. Tysoe, W. T.; Nyberg, G. L.; Lambert, R. M. Photoelectron Spectroscopy and Heterogeneous Catalysis: Benzene and Ethylene from Acetylene on Palladium(111). *Surf. Sci.* **1983**, *135*, 128–146.
4. Patterson, C. H.; Lambert, R. M. Molecular Mechanisms in the Cyclotrimerization of Acetylene to Benzene on Palladium(111). *J. Phys. Chem.* **1988**, *92*, 1266–1270.
5. Tysoe, W. T.; Nyberg, G. L.; Lambert, R. M. Low Temperature Catalytic Chemistry of the Pd(111) Surface: Benzene and Ethylene from Acetylene. *J. Chem. Soc. Chem. Commun.* **1983**, *289*, 623–625.
6. Ormerod, R. M.; Lambert, R. M. Two Dimensional Compression and Catalysis: Acetylene → Benzene Conversion Induced by Spectator Nitric Oxide. *Surf. Sci. Lett.* **1990**, *225*, L20–L24.
7. Morkel, M.; Rupprechter, G.; Freund, H.-J. Ultrahigh Vacuum and High-Pressure Coadsorption of CO and H_2 on Pd(111): A Combined SFG, TDS, and LEED Study. *J. Chem. Phys.* **2003**, *119*, 10853–10866.
8. Montano, M.; Bratlie, K.; Salmeron, M.; Somorjai, G. A. Hydrogen and Deuterium Exchange on Pt(111) and Its Poisoning by Carbon Monoxide Studied by Surface Sensitive High-Pressure Techniques. *J. Am. Chem. Soc.* **2006**, *128*, 13229–13234.
9. Wintterlin, J.; Völkening, S.; Janssens, T. V. W.; Zambelli, T.; Ertl, G. Atomic and Macroscopic Reaction Rates of a Surface-Catalyzed Reaction. *Science* **1997**, *278*, 1931–1934.
10. Tang, D. C.; Hwang, K. S.; Salmeron, M.; Somorjai, G. A. High Pressure Scanning Tunneling Microscopy Study of CO Poisoning of Ethylene Hydrogenation on Pt(111) and Rh(111) Single Crystals. *J. Phys. Chem. B* **2004**, *108*, 13300–13306.
11. Rider, K. B.; Hwang, K. S.; Salmeron, M.; Somorjai, G. A. High-Pressure (1 Torr) Scanning Tunneling Microscopy (STM) Study of the Coadsorption and Exchange of CO and NO on the Rh(111) Crystal Face. *J. Am. Chem. Soc.* **2002**, *124*, 5588–5593.
12. Kok, G. A.; Nordermeer, A.; Nieuwenhuys, B. E. Decomposition of Methanol and the Interaction of Coadsorbed Hydrogen and Carbon Monoxide on a Pd(111) Surface. *Surf. Sci.* **1983**, *135*, 65–80.
13. Cerdá, J. I.; Santos, B.; Herranz, T.; Peurta, J. M.; de la Figuera, J.; McCarthy, K. F. CO-Assisted Subsurface Hydrogen Trapping in Pd(111) Films. *J. Phys. Chem. Lett.* **2012**, *3*, 87–91.
14. Rose, M. K.; Mitsui, T.; Dunphy, J.; Borg, A.; Ogletree, D. F.; Salmeron, M.; Sautet, P. Ordered Structures of CO on Pd(111) Studied by STM. *Surf. Sci.* **2002**, *512*, 48–60.
15. Demchenko, D. O.; Sacha, G. M.; Salmeron, M.; Wang, L.-W. Interactions of Oxygen and Hydrogen on Pd(111) Surface. *Surf. Sci.* **2008**, *602*, 2552–2557.
16. Mitsui, T.; Rose, M. K.; Fomin, E.; Ogletree, D. F.; Salmeron, M. Coadsorption and Interactions of O and H on Pd(111). *Surf. Sci.* **2002**, *511*, 259–266.
17. Seitsonen, A. P.; Kim, Y. D.; Schwegmann, S.; Over, H. Comprehensive Characterization of the (2 × 2)-O and the CO-Induced ($\sqrt{3} \times \sqrt{3}$)R30°-O Overlayers on Pd(111). *Surf. Sci.* **2000**, *468*, 176–186.
18. Calaza, F.; Stacchiola, D.; Neurock, M.; Tysoe, W. T. Coverage Effects on the Palladium-Catalyzed Synthesis of Vinyl Acetate: Comparison between Theory and Experiment. *J. Am. Chem. Soc.* **2010**, *132*, 2202–2207.
19. Campbell, C. T.; Ernst, K.-H. Forward and Reverse Water-Gas Shift Reactions on Model Copper Catalysts; Kinetics and Elementary Steps. In *ACS Symposium Series: Surface Science of Catalysis, In Situ Probes and Reaction Kinetics*; Dwyer, D. J., Hoffmann, F. M., Eds.; American Chemical Society: Washington D.C., 1992; pp 130—142.
20. Lewis, E. A.; Le, D.; Murphy, C. J.; Jewell, A. D.; Mattera, M. F. G.; Liriano, M. L.; Rahman, T. S.; Sykes, E. C. H. Dissociative Hydrogen Adsorption on Close-Packed Nanoparticle Surfaces. *J. Phys. Chem. C* **2012**, *116*, 25868–25873.
21. Inderwildi, O. R.; Jenkins, S. J.; King, D. A. Fischer–Tropsch Mechanism Revisited: Alternative Pathways for the Production of Higher Hydrocarbons from Synthesis Gas. *J. Phys. Chem. C* **2008**, *112*, 1305–1307.
22. Inderwildi, O. R.; King, D. A.; Jenkins, S. J. Fischer–Tropsch Synthesis of Liquid Fuels: Learning Lessons from Homogeneous Catalysis. *Phys. Chem. Chem. Phys.* **2009**, *11*, 11110–11112.
23. Ojeda, M.; Nabar, R.; Nilekar, A. U.; Ishikawa, A.; Mavrikakis, M.; Iglesia, E. CO Activation Pathways and the Mechanism of Fischer–Tropsch Synthesis. *J. Catal.* **2010**, *272*, 287–297.
24. Zhao, Y.-H.; Sun, K.; Ma, X.; Liu, J.; Sun, D.; Su, H.-Y.; Li, W.-X. Carbon Chain Growth by Formyl Insertion on Rhodium and Cobalt Catalysts in Syngas Conversion. *Angew. Chem., Int. Ed.* **2011**, *50*, 5335–5338.
25. de la Figuera, J.; Prieto, J. E.; Ocal, C.; Miranda, R. Scanning-Tunneling-Microscopy Study of the Growth of Cobalt on Cu(111). *Phys. Rev. B* **1993**, *47*, 13043–13046.
26. de la Figuera, J.; Prieto, J. E.; Kostka, G.; Müller, S.; Ocal, C.; Miranda, R.; Heinz, K. Crystallography and Morphology of the Early Stages of the Growth of Co/Cu(111) by LEED and STM. *Surf. Sci.* **1996**, *349*, L139–L145.
27. Negulyaev, N. N.; Stepanyuk, V. S.; Bruno, P.; Diekhöner, L.; Wahl, P.; Kern, K. Bilayer Growth of Nanoscale Co Islands on Cu(111). *Phys. Rev. B* **2008**, *77*, 1254371–1254377.
28. Sicot, M.; Kurnosikov, O.; Adam, O. A. O.; Swagten, H. J. M.; Koopmans, B. STM-Induced Desorption of Hydrogen from Co Nanoislands. *Phys. Rev. B* **2008**, *77*, 0354171–0354177.
29. Sicot, M.; Kurnosikov, O.; Swagten, H. J. M.; Koopmans, B. Hydrogen Superstructures on Co Nanoislands and Cu(111). *Surf. Sci.* **2008**, *602*, 3667–3673.
30. Duś, R.; Lisowski, W. Adsorption of Hydrogen on Evaporated Cobalt Films. *Surf. Sci.* **1976**, *61*, 635–645.
31. Bridge, M. E.; Comrie, C. M.; Lambert, R. M. Hydrogen Chemisorption and the Carbon Monoxide-Hydrogen Interaction on Cobalt (0001). *J. Catal.* **1979**, *58*, 28–33.
32. Butterfield, M. T.; Crapper, M. D.; Noakes, T. C. Q.; Bailey, P.; Jackson, G. J.; Woodruff, D. P. Structure of Ultrathin Films

of Co on Cu(111) from Normal-Incidence X-Ray Standing Wave and Medium-Energy Ion Scattering Measurements. *Phys. Rev. B* **2000**, *62*, 16984–16994.
33. Pietzsch, O.; Kubetzka, A.; Bode, M.; Wiesendanger, R. Spin-Polarized Scanning Tunneling Spectroscopy of Nanoscale Cobalt Islands on Cu(111). *Phys. Rev. Lett.* **2004**, *92*, 0572021–0572024.
34. Pietzsch, O.; Okatov, S.; Kubetzka, A.; Bode, M.; Heinze, S.; Lichtenstein, A.; Wiesendanger, R. Spin-Resolved Electronic Structure of Nanoscale Cobalt Islands on Cu(111). *Phys. Rev. Lett.* **2006**, *96*, 2372031–2372034.
35. Rastei, M. V.; Heinrich, B.; Limot, L.; Ignatiev, P. A.; Stepanyuk, V. S.; Bruno, P.; Bucher, J. P. Size-Dependent Surface States of Strained Cobalt Nanoislands on Cu(111). *Phys. Rev. Lett.* **2007**, *99*, 2461021–2461024.
36. Oka, H.; Ignatiev, P. A.; Wedekind, S.; Rodary, G.; Niebergall, L.; Stepanyuk, V. S.; Sander, D.; Kirschner, J. Spin-Dependent Quantum Interference Within a Single Magnetic Nanostructure. *Science* **2010**, *327*, 843–846.
37. Lewis, E. A.; Jewell, A. D.; Kyriakou, G.; Sykes, E. C. H. Rediscovering Cobalt's Surface Chemistry. *Phys. Chem. Chem. Phys.* **2012**, *14*, 7215–7224.
38. Kitakami, O.; Sato, H.; Shimada, Y.; Sato, F.; Tanaka, M. Size Effect on the Crystal Phase of Cobalt Fine Particles. *Phys. Rev. B* **1997**, *56*, 13849–13853.
39. Van Helden, P.; van den Berg, J.-A.; Westrate, C. J. Hydrogen Adsorption on Co Surfaces: A Density Functional Theory and Temperature Programmed Desorption Study. *ACS Catal.* **2012**, *2*, 1097–1107.
40. Bridge, M. E.; Comrie, C. M.; Lambert, R. M. Chemisorption Studies on Cobalt Single Crystal Surfaces, I. Carbon Monoxide on Co(0001). *Surf. Sci.* **1977**, *67*, 393–404.
41. Lahtinen, J.; Vaari, J.; Kauraala, K. Adsorption and Structure Dependent Desorption of CO on Co(0001). *Surf. Sci.* **1998**, *418*, 502–510.
42. Cheng, Z.; Luo, M.; Wyrick, J.; Sun, D.; Kim, D.; Zhu, Y.; Lu, W.; Kim, K.; Einstein, T. L.; Bartels, L. Power of Confinement: Adsorbate Dynamics on Nanometer-Scale Exposed Facets. *Nano Lett.* **2010**, *10*, 3700–3703.
43. Cheng, Z.; Wyrick, J.; Luo, M.; Sun, D.; Kim, D.; Zhu, Y.; Lu, W.; Kim, K.; Einstein, T. L.; Bartels, L. Adsorbates in a Box: Titration of Substrate Electronic States. *Phys. Rev. Lett.* **2010**, *105*, 0661041–0661044.
44. Braun, W.; Steinrück, H.-P.; Held, G. The Surface Geometry of Carbonmonoxide and Hydrogen Co-Adsorbed on Ni{111}. *Surf. Sci.* **2005**, *574*, 193–204.
45. Kirstein, W.; Krüger, B.; Theime, F. CO Adsorption Studies on Pure and Ni-Covered Cu(111) Surfaces. *Surf. Sci.* **1986**, *176*, 505–529.
46. Jewell, A. D.; Kyran, S. J.; Rabinovich, D.; Sykes, E. C. H. Effect of Head-Group Chemistry on Surface-Mediated Molecular Self-Assembly. *Chem.—Eur. J.* **2012**, *18*, 7169–7178.
47. Schrader, M. E. Spreading Pressure in the Young Equation and Intermolecular Force Theory. *Langmuir* **1993**, *9*, 1959–1961.
48. Pick, Š. Density-Functional Theory Study of the Compressed $(2\sqrt{3} \times 2\sqrt{3})$R30°-CO Overlayer on the Ferromagnetic Co(0001) Surface. *Surf. Sci.* **2012**, *606*, 692–696.
49. Jewell, A. D.; Peng, G.; Mattera, M. F. G.; Lewis, E. A.; Murphy, C. J.; Kyriakou, G.; Mavrikakis, M.; Sykes, E. C. H. Quantum Tunneling Enabled Self-Assembly of Hydrogen Atoms on Cu(111). *ACS Nano* **2012**, *6*, 10115–10121.
50. Blöchl, P. E. Projector Augmented-Wave Method. *Phys. Rev. B* **1994**, *50*, 17953–17979.
51. Kresse, G.; Joubert, D. From Ultrasoft Pseudopotentials to the Projector Augmented-Wave Method. *Phys. Rev. B* **1999**, *59*, 1758–1775.
52. Kresse, G.; Furthmüller, J. Efficient Iterative Schemes for *ab Initio* Total-Energy Calculation Using a Plane-Wave Basis Set. *Phys. Rev. B* **1996**, *54*, 11169–11186.
53. Perdew, J. P.; Burke, K.; Ernzerhof, M. Generalized Gradient Approximation Made Simple. *Phys. Rev. Lett.* **1996**, *77*, 3865–3868.
54. Bengtsson, L. Dipole Correction for Surface Supercell Calculations. *Phys. Rev. B* **1999**, *59*, 12301–12304(1999).
55. Reuter, K.; Scheffler, M. Composition, Structure, and Stability of RuO_2(110) as a Function of Oxygen Pressure. *Phys. Rev. B* **2001**, *65*, 0354061–03540611.
56. Feibelman, P. J.; Hammer, B.; Nørskov, J. K.; Wagner, F.; Scheffler, M.; Stumpf, R.; Watwe, R.; Dumesic, J. The CO/Pt(111) Puzzle. *J. Phys. Chem. B* **2001**, *105*, 4018–4025.
57. Dudarev, S. L.; Botton, G. A.; Savrasov, S. Y.; Humphreys, C. J.; Sutton, A. P. Electron-Energy-Loss Spectra and the Structural Stability of Nickel Oxide: An LSDA+U Study. *Phys. Rev. B* **1998**, *57*, 1505–1509.
58. Moler, E. J.; Kellar, S. A.; Huff, W. R. A.; Hussain, Z.; Chen, Y.; Shirley, D. A. Spatial Structure Determination of $(\sqrt{3}x\sqrt{3})$R30° and (1.5 × 1.5)R18° CO or Cu(111) Using Angle-Resolved Photoemission Extended Fine Structure. *Phys. Rev. B* **1996**, *54*, 10862–10868.
59. Vollmer, S.; Witte, G.; Wöll, C. Determination of Site Specific Adsorption Energies of CO on Copper. *Catal. Lett.* **2001**, *77*, 97–101.